On the Role of the African Topography in the South Asian Monsoon

HO-HSUAN WEI AND SIMONA BORDONI

California Institute of Technology, Pasadena, California

(Manuscript received 3 July 2015, in final form 11 May 2016)

ABSTRACT

The Somali jet, a strong low-level cross-equatorial flow concentrated in a narrow longitudinal band near the coast of Somalia, is a key feature of the South Asian monsoon (SAM) circulation. Previous work has emphasized the role of the East African highlands in strengthening and concentrating the jet. However, the fundamental dynamics of the jet remains debated, as does its relation to the SAM precipitation. In this study, numerical experiments with modified topography over Africa are conducted with the GFDL atmospheric model, version 2.1 (AM2.1), general circulation model (GCM) to examine the influence of topography on the Somali jet and the SAM precipitation. It is found that when the African topography is removed, the SAM precipitation moderately increases in spite of a weakening of the cross-equatorial Somali jet. The counterintuitive precipitation increase is related to lower-level cyclonic wind anomalies, and associated meridional moisture convergence, which develop over the Arabian Sea in the absence of the African topography. Potential vorticity (PV) budget analyses along particle trajectories show that this cyclonic anomaly primarily arises because, in the absence of the blocking effect by the African topography and with weaker cross-equatorial flow, air particles originate from higher latitudes with larger background planetary vorticity and thus larger PV.

1. Introduction

The South Asian monsoon (SAM) is the southern part of the Asian monsoon system, the largest-scale monsoon in Earth's atmosphere. The monsoon brings rain that is concentrated in the summer to densely populated and rapidly growing regions, such as India and neighboring countries. Traditionally, the SAM has been interpreted as a large-scale sea-breeze circulation driven by contrast in thermal properties between the Indian subcontinent and the surrounding ocean (e.g., Webster 1987; Meehl 1994; Wu et al. 2012). However, recent theoretical advances suggest that the SAM should be more generally viewed as the regional manifestation of the seasonal migration of the intertropical convergence zone (ITCZ) into the summer subtropical continents (e.g., Gadgil 2003). The associated thermally direct circulation is characterized by ascending motion in the summer hemisphere subtropics, opposite cross-equatorial flows at lower and upper levels, and descending motion in the winter hemisphere (e.g., Nie et al. 2010), giving rise to a reversed meridional temperature gradient and, by thermal wind balance, an easterly vertical wind shear in the summer hemisphere (e.g., Li and Yanai 1996). At lower levels, westerly winds dominate in the summer hemisphere over the Indian Ocean, consistent with the Coriolis force on the cross-equatorial flow approximately balancing the drag in near-surface zonal winds (e.g., Bordoni and Schneider 2008), while easterlies develop at upper levels. The strong precipitation, the displacement into the Northern Hemisphere (NH) of the upper-tropospheric temperature maximum, and reversal of lower-level winds from easterly to westerly over the Indian Ocean in the NH are all distinctive features of the SAM in boreal summer.

Upstream of the lower-level westerlies, a strong cross-equatorial jet develops near the east coast of Africa. This jet, referred to in the literature as the Somali jet, flows along the East African highlands (EAHs), having a core located at about 1.5 km above sea level, equatorial mean wind speed of around $25\,m\,s^{-1}$, and maximum wind speed as large as $50\,m\,s^{-1}$ (Findlater 1969). The Somali jet is estimated to contribute up to half of the mass flux crossing the equator during the Asian summer monsoon season. After crossing the equator and

Corresponding author address: Ho-Hsuan Wei, California Institute of Technology, 1200 E. California Blvd., MC131-24, Pasadena, CA 91125.
E-mail: hwei@caltech.edu

DOI: 10.1175/JAS-D-15-0182.1

turning eastward in the Arabian Sea, the jet brings into the Indian subcontinent moisture from the warm ocean, with around 60%–80% of the moisture estimated to originate from the Southern Hemisphere (SH) (Hoskins and Rodwell 1995).

The Somali jet results from cross-equatorial flow developing in response to the ITCZ displacement in the NH subtropics, and its dynamics has been described as analogous to those of western boundary currents in the ocean (e.g., Anderson 1976). The EAHs have been argued to be essential for the spatial concentration and strength of the cross-equatorial flow. Krishnamurti et al. (1976) used a one-level primitive equation model to show that the East African and Madagascar mountains, the land–sea contrast, and the beta effect are all necessary to simulate a Somali jet similar to what is seen in observations. Subsequent studies have explored the response of linear models with prescribed diabatic heating and have argued that a western boundary (provided by the EAHs) is necessary to develop a concentrated cross-equatorial flow (e.g., Paegle and Geisler 1986; Sashegyi and Geisler 1987). Rodwell and Hoskins (1995, hereafter RH95) extended these results to a nonlinear, hydrostatic, primitive equation model with linear drag in the lowest two levels and specified orography and diabatic heating. Their analysis shows how the combination of high terrain over East Africa and greater friction there acts as a positive tendency to potential vorticity (PV) that partially cancels the negative PV of air crossing the equator from the SH and allows the flow to concentrate in a jet and remain in the NH, rather than curving back southward and returning into the SH.

Interest in the fundamental dynamics of the Somali jet is motivated by its possible impact on the SAM precipitation through the associated moisture transport. Some early observational studies do support a positive correlation between the strength of the Somali jet and the rainfall intensity over western India (e.g., Findlater 1969; Halpern and Woiceshyn 2001). However, no comprehensive observational study has provided further support to the existence of such robust correlation on scales from intraseasonal to interannual using recent higher-resolution data. The only multiyear study based on reanalysis (Boos and Emanuel 2009) indicates that the rapid onset of the SAM is not associated with a rapid strengthening of the Somali jet. This suggests that the relationship between the lower-level cross-equatorial jet and the monsoonal precipitation might be more subtle than generally thought. This is confirmed by recent modeling studies, which show that the removal of the African topography in fact results in an increase rather than a decrease of the monsoonal precipitation over India, despite a weakening of the Somali jet (Chakraborty et al. 2002, 2006, 2009; Slingo et al. 2005).

This discussion highlights how important questions on the impact of the African orography on the SAM remain outstanding: 1) How does topography over Africa affect the strength and spatial structure of the Somali jet? 2) What is the relationship between the cross-equatorial flow and its downstream westerly extension over the Arabian Sea? 3) How are topographically induced changes in lower-level meridional and zonal flow related to the SAM precipitation? In this paper, we will address these questions by performing simulations with a comprehensive general circulation model (GCM) with modified topography over Africa and the Arabian Peninsula. The GCM experiments and analysis methods are described in section 2. In section 3, we explore how the Somali jet and the precipitation over the SAM region respond to the removal of the African topography. The dynamics of these changes is explored more in depth and linked to changes in the PV and the larger-scale monsoonal circulation in section 4. In section 5, we present results from an additional simulation, in which we remove both the African and Arabian topography, to understand how the absence of an extended topographical wall from Africa into Arabia might affect the monsoon. Conclusions follow in section 6.

2. Methods

The simulations in this study are performed with the Geophysical Fluid Dynamics Laboratory (GFDL) Atmospheric Model, version 2.1 (AM2.1; Anderson et al. 2004). AM2.1 uses a finite-volume dynamical core with horizontal resolution of 2.5° longitude and 2.0° latitude and 24 vertical levels. Climatologically fixed sea surface temperatures (SSTs) derived from 2° × 2° 49-yr (1950–98) monthly mean of Reynolds reconstructed historical SST analysis (Smith et al. 1996) are used as the lower boundary condition. The convection scheme is the relaxed Arakawa–Schubert scheme.

In this study, we primarily discuss two simulations: A control (CTL) simulation where full global topography is retained (Fig. 1a) and an experiment simulation in which topography over Africa is removed (NoAf). In the NoAf experiment, topography is removed in the regions 0–35°N, 20°W–35°E and 40°S–15°N, 10°–50°E (Fig. 1b). The topographic height of the grid points right outside the edge of these boxes is halved to allow for a smoother transition. In section 5, we also briefly discuss an additional experiment, NoAfArab, in which together with topography over Africa we also remove the Arabian topography. More precisely, in the NoAfArab experiment, topography is removed from

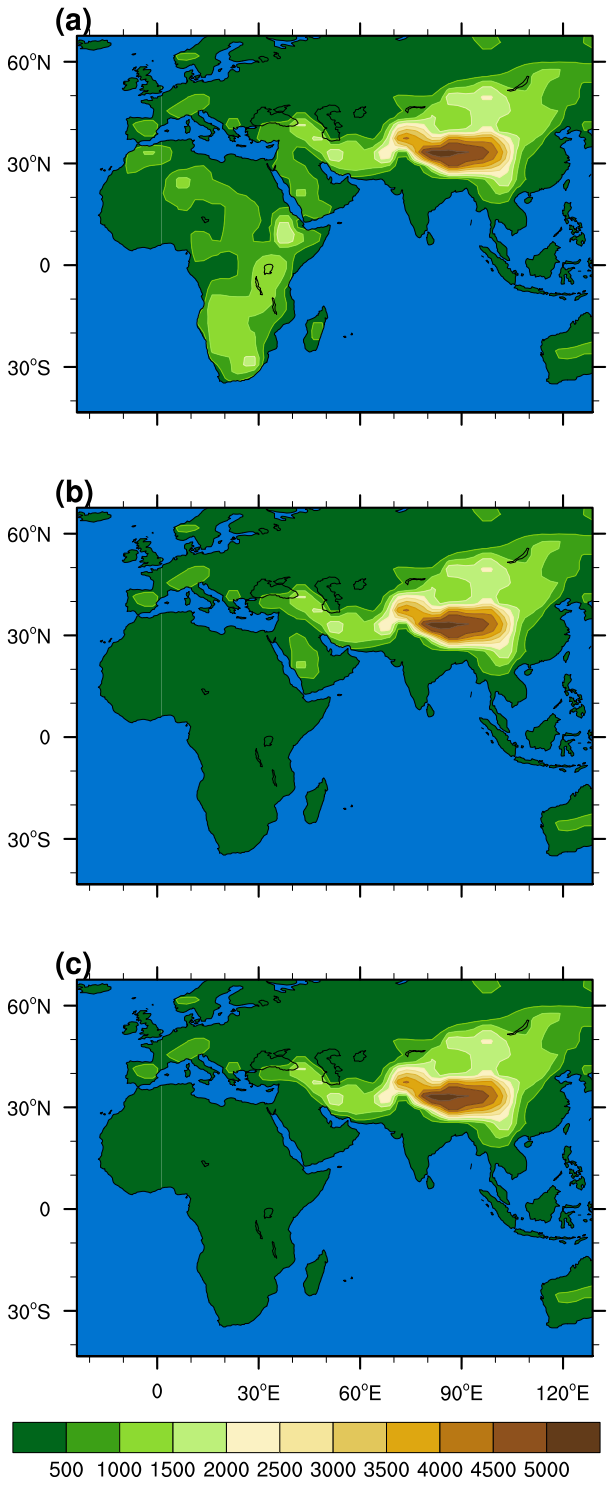

FIG. 1. Surface height (m) configuration in the (a) CTL, (b) NoAf, and (c) NoAfArab experiments.

0°–35°N, 20°W–40°E; 40°S–15°N, 10°–50°E; 15°–30°N, 40°–47°E; and 15°–25°N, 47°–55°E (Fig. 1c). In all these experiments, the orographic gravity wave drag is modified accordingly to modified topography.

The initial conditions for all three experiments are derived from a 1-yr simulation with standard topography. After the topography height is changed following the 1-yr simulation, the experiments are integrated for 19 yr, and the analyses discussed below are based on the last 10 simulated years.

Large-scale budgets, such as the moisture and PV budgets, are analyzed to shed light into mechanisms that are implicated in the precipitation and circulation response to the change of topography. We also perform trajectory analyses to explore how topography, possibly through blocking or changes in the Somali jet, impacts the trajectories of air parcels reaching the Indian region and to more carefully analyze the PV budget from a material perspective. Three-hour wind field data in pressure coordinates are used to compute backward and forward trajectories. The integration time step is 3-h as the data output. For each integration, we use the wind field at the time of calculation, so that the wind field used in the integration is updated at every calculated time step. Once the trajectories have been computed, other variables, including the different terms in the PV analysis, as described in detail in section 4, are interpolated along the paths. Please note that trajectories are being computed using the three-dimensional (3D) wind field resolved by the GCM at the grid scale. In regions where convection is active, the resolved mean vertical velocity might underestimate vertical motions due to subgrid-scale convective processes.

To consider the conditions representative of the JJA average, which is what we show throughout the paper, eight different integration-starting dates are chosen within July and August at selected locations (e.g., 15, 20, 25, and 30 July and 5, 10, 15, and 20 August) for the trajectory analyses. In the PV budget analysis, we average these eight integrations to show average summertime trajectories. The spread of the eight trajectories for the different integration-starting dates increases with integration time, but the trajectories all have similar patterns (not shown).

3. Impact of the African topography on the Somali jet and SAM precipitation

The CTL model integration with standard topography produces a SAM with large-scale precipitation and circulation patterns similar to those found in observations (Fig. 2). The model precipitation exhibits some bias, with stronger maxima near the western Ghats and the

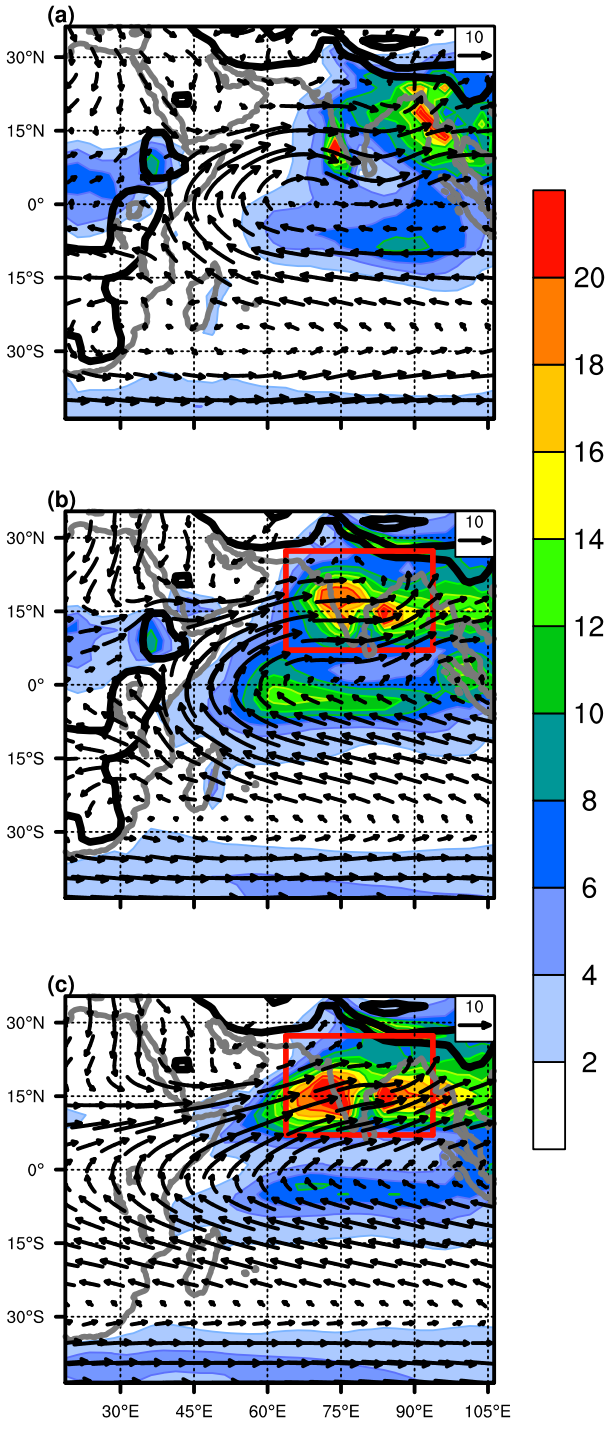

FIG. 2. JJA precipitation (shading, mm day^{-1}) and 850-hPa winds (vectors, m s^{-1}) in (a) observations, (b) the CTL, and (c) NoAf experiments. In (a), precipitation is from GPCP v2.2 and winds are from the NCEP reanalysis. Thick black lines indicate the surface height in each simulation (from 1000 to 5000 m, contour interval 2000 m). The red rectangle indicates the "Indian region," for which accumulated precipitation in the model experiments is shown in Fig. 5a.

southerly Himalayas and a weaker and southward shifted maximum over the Bay of Bengal. Other GCMs feature similar simulated bias in this region (e.g., Boos and Kuang 2010). The cross-equatorial Somali jet, whose response to topography modifications is a primary focus in this paper, is also well captured. The reasonable agreement between the CTL experiment and the observations gives us confidence on the use of AM2.1 as a valid tool to study the impact of the African topography on the SAM.

When topography over Africa is removed in AM2.1, we find that the meridional cross-equatorial flow in the core of the Somali jet weakens, with a reduction of ~30% of the maximum jet strength (Fig. 3). While not explicitly discussed there, this weakening appears to be in agreement with simulation results in previous studies (Chakraborty et al. 2002, 2006, 2009; Slingo et al. 2005). A pressure–longitude cross section at the equator shows that the maximum reduction is at around 800 hPa, slightly above the simulated maximum in CTL at 850 hPa. Additionally, in the NoAf experiment, the cross-equatorial flow spreads over the African continent, and the jet core moves to lower levels and weakens. This finding confirms that the African topography helps accelerate and spatially concentrate the Somali jet. Interestingly, we find that the removal of the African topography causes a positive meridional wind anomaly over the Arabian Sea north of the equator, where climatological winds are primarily westerlies (Fig. 4a and Figs. 2b,c). As discussed below, this positive anomaly has an unexpected and important impact on the SAM precipitation.

The weakening of the cross-equatorial flow in the Somali jet core region in the absence of topography over Africa might support the expectation of a similar decrease in monsoonal precipitation, possibly because of decreased moisture transport. Counterintuitively, we find that precipitation increases almost everywhere in the Indian region, with largest anomalies just west of the Indian subcontinent over the Arabian Sea and smaller anomalies over the Bay of Bengal (Figs. 2b,c and Fig. 5b). The "Indian region" here is defined as the broad area within 7.07°–27.3°N, 63.75°–93.75°E (shown by the red rectangle in Figs. 2b,c and following figures), which includes the Indian subcontinent and neighboring oceans, where precipitation maxima are found in the CTL experiment (Fig. 2). The accumulated precipitation in this region, representative of the larger-scale SAM, is shown in Fig. 5a for the different numerical experiments: in the NoAf experiment, area-averaged JJA accumulated precipitation increases by ~16% compared to the CTL experiment. In the following, we primarily focus on mechanisms responsible for the precipitation response over the Arabian Sea, which are more clearly

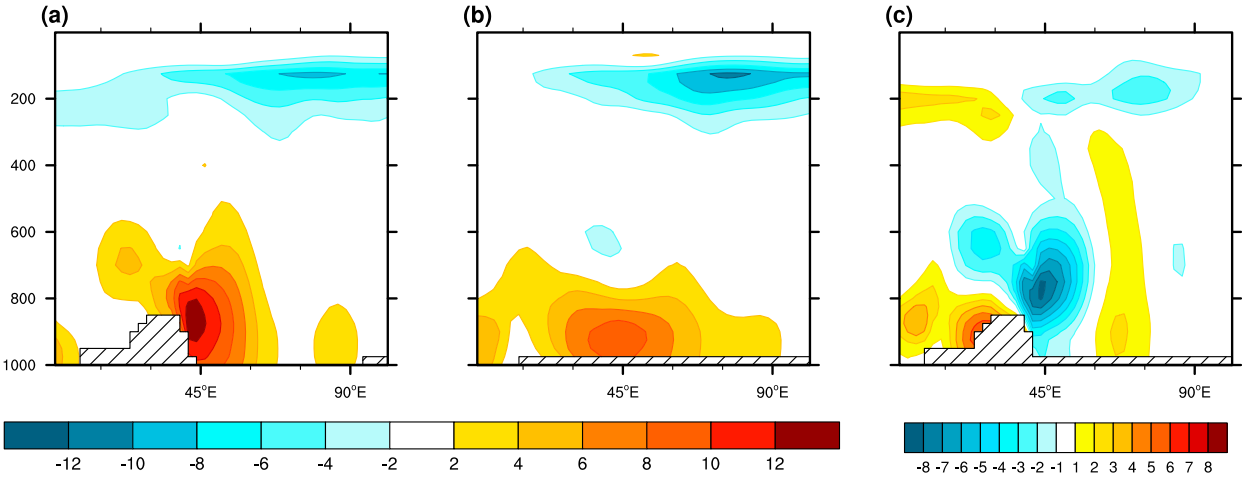

FIG. 3. Equatorial (1°S–1°N) pressure–longitude cross section of the JJA-average meridional wind ($m\,s^{-1}$) in (a) CTL, (b) NoAf, and (c) the difference between the two.

linked to possible changes in the Somali jet, and associated moisture transport, and have been the focus of previous studies (e.g., Chakraborty et al. 2002, 2006, 2009).

These results therefore demonstrate how changes in the strength of the Somali jet in response to modified topography are not linearly correlated to changes in the SAM precipitation. This is consistent with Boos and Emanuel (2009), who show how in the annual cycle the rapid strengthening of the wind over the Arabian Sea at monsoon onset is not accompanied by similarly rapid changes in the cross-equatorial mass transport in the core of the jet near the EAHs (between 38.75° and 48.75°E). They found that these rapid SAM wind changes are instead accompanied by a rapid strengthening of the cross-equatorial mass transport in the periphery of the jet (between 48.75° and 71.25°E). This suggests that the maximum speed of the cross-equatorial jet, which is influenced by the existence of the African topography, might not be directly related to the SAM precipitation. Following the procedure in Boos and Emanuel (2009), we analyze separately changes in the cross-equatorial mass flux in the topographically bound core cross-equatorial flow and in its oceanic periphery region. As shown in Fig. 6, in the NoAf experiment, the cross-equatorial mass flux decreases solely in the core region and remains largely unchanged in the periphery. This suggests that even in the absence of the African topography, the cross-equatorial mass flux in the periphery region transports sufficient moisture to sustain the monsoon and prevents significant decreases in its precipitation.

While the removal of the African topography does not significantly alter the large-scale patterns of the SAM, it is accompanied by an increase in the overall accumulated precipitation that is larger than the standard deviation (10%) associated with the observed monsoon interannual variability and leads to nonnegligible regional changes. We interpret these regional changes using the moisture budget, which relates the net precipitation (precipitation minus evaporation; $P - E$) to the vertically integrated moisture flux convergence. Calling δ the difference between the NoAf and CTL experiments, and decomposing changes in the moisture flux convergence into changes due to winds (the dynamic components, including the convergence and advection terms) and changes due to moisture (the thermodynamic component) as done by a number of previous studies (e.g., Clement et al. 2004; Held and Soden 2006; Walker et al. 2015), we can write

$$\delta\overline{P} \approx \delta\overline{E} - \langle \overline{q}\nabla\cdot\delta\overline{\mathbf{v}}\rangle - \langle \delta\overline{\mathbf{v}}\cdot\nabla\overline{q}\rangle - \langle \nabla\cdot[(\delta\overline{q})\overline{\mathbf{v}}]\rangle, \qquad (1)$$

where q represents the specific humidity, $\mathbf{v}$ represents the horizontal wind field, $\langle\cdot\rangle$ represents a mass-weighted vertical integral [i.e., $\int(\cdot)\,dp/g$] and $\overline{(\cdot)}$ represents a time average. The first term in the right-hand side is the change in evaporation, the second term the dynamic convergence term, the third term the dynamic advection term, and the last term the thermodynamic term.

Except for evaporation, which is negligible, the contribution of all terms in Eq. (1) to precipitation changes are shown in Fig. 7. The residual term is small relative to the other terms, especially compared to the δP term. This small residual also includes the quadratic term, which is due to covariations in changes of moisture and winds, and the surface term, which is due to the additional vertical levels (i.e., pressure interval) in the NoAf experiment where topography is removed. This surface term can be explicitly computed, and we find that its contribution to the moisture flux convergence in the area where

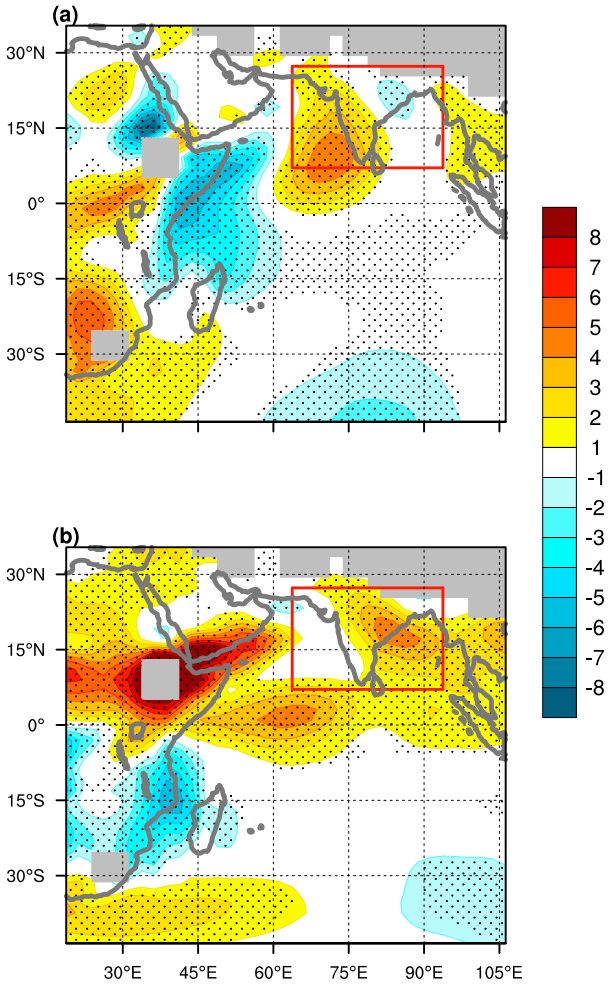

FIG. 4. Anomalous (NoAf–CTL) (a) meridional and (b) zonal wind at 850 hPa (m s^{-1}). The gray shading indicates regions with no data below 850 hPa. The red box is as in Fig. 2. Stippling shows regions where the wind anomalies are statistically significant at the 95% level.

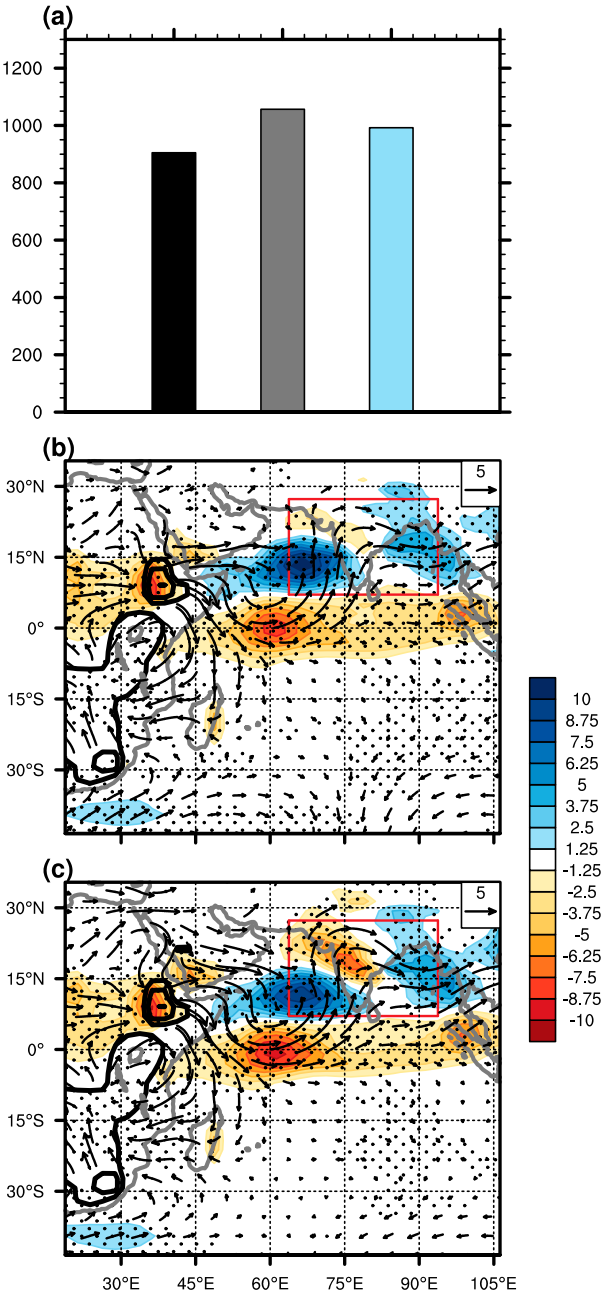

FIG. 5. (a) Accumulated JJA precipitation (mm) averaged over the Indian region [(b) red rectangle] in the CTL (black), NoAf (gray), and NoAfArab (light blue) experiments. Anomalous JJA precipitation (shading, mm day^{-1}) and 850-hPa winds (vectors, m s^{-1}) for (b) NoAf–CTL and (c) NoAfArab–CTL. Thick black lines indicate the surface pressure anomalies (contour interval 50 hPa) and, hence, topography difference between the two experiments. Stippling shows regions where anomalies are statistically significant at the 95% level.

topography is removed is small, despite a local increase in moisture there (not shown). Consistent with Chakraborty et al. (2002, 2006, 2009), we find that the largest contribution comes from the dynamic convergence component, that is, changes in precipitation are primarily accounted for by changes in wind convergence. Chakraborty et al. (2009) suggest that in the absence of blocking by the African topography, the westerly flow over Africa would extend eastward into the Arabian Sea and increase the westerlies there. This in turn would favor an increased wind and moisture convergence as the flow approaches the Indian subcontinent. We test this hypothesis by examining how both the westerly flow and air parcel trajectories are modified in the absence of the African topography. When comparing forward trajectories for particles originating over Africa at 850 hPa in the CTL (Fig. 8a) and NoAf (Fig. 8b) experiments, we see that in the absence of the African topography air particles can indeed flow past Africa and move into the Indian region. Also, in our simulations, the zonal wind does increase

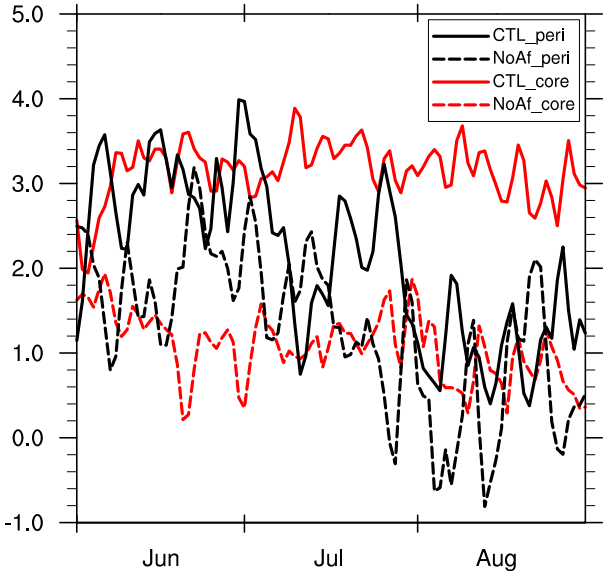

FIG. 6. Time evolution of the cross-equatorial (5°S–5°N) mass flux (10^{10} kg s^{-1}), with red and black lines showing values integrated over the core (38.75°–48.75°E) and periphery (48.75°–71.25°E) of the jet region, respectively. The solid lines show the CTL, while the dashed lines show the NoAf experiment.

near the region in which topography is removed and over the equatorial Indian Ocean (Fig. 4b). This suggests that indeed the African topography blocks air from Africa and weakens the westerlies. However, the stronger zonal wind does not extend into the Arabian Sea, to the west of the Indian subcontinent, where the precipitation response to the topography removal is the largest. After further decomposing the horizontal convergence in the dynamic convergence term into zonal and meridional components in the moisture budget [Eq. (1)], we find that the enhanced precipitation results primarily from increased meridional wind convergence, rather than stronger zonal wind convergence as proposed by Chakraborty et al. (2009) (Figs. 7e,f). This stronger meridional moisture convergence is associated with the development of a larger-scale cyclonic circulation anomaly over the Arabian Sea (Fig. 5b). Mechanisms driving this cyclonic anomaly are explored more in detail in the next section.

4. Impact of the African topography on the larger-scale circulation

a. *Stationary wave pattern*

The cyclonic anomaly developing over the Arabian Sea in response to the removal of the African topography and the anticyclonic anomalies in its upstream and downstream are indicative of a wavelike pattern. A similar wavelike pattern is also seen in the simulations of Slingo et al. (2005), who suggest a possible link between the stationary wave response to the African topography and changes in the SAM precipitation as the topography is removed. This stationary wave pattern can be qualitatively understood as a direct response to the weakening of the cross-equatorial meridional flow as topography is removed: a weakening of the cross-equatorial southerly wind at its core along the coast of Africa at around 8°N and 50°E would be accompanied by cyclonic anomalies to its east at around 50°–70°E and anticyclonic anomalies to its west at around 40°–50°E, consistent with what seen in our simulations (Fig. 9a). However, as already extensively discussed in RH95, a full consideration of the PV budget can provide a quantitative understanding of the flow properties and PV dynamics in the downstream of the cross-equatorial meridional flow. In the following subsection, we present PV budget analyses following trajectories to develop a more mechanistic understanding of the cyclonic anomaly over the Arabian Sea in the NoAf experiment.

b. *PV dynamics of the Somali jet and its relation with the SAM precipitation*

As discussed in detail in the previous subsection and as shown in Fig. 9a, a cyclonic circulation anomaly (i.e., the difference between the NoAf and CTL experiments) exists to the west of India over the Arabian Sea. A region of positive PV anomaly is also located there. In section 3, we have shown how, as topography is removed, precipitation increases mainly over the ocean just west of the Indian subcontinent (Fig. 5b), primarily in association with anomalous meridional wind convergence (Fig. 7f). The increased meridional wind convergence is collocated and related to the southerly flow on the eastern flank of the cyclonic anomaly over the Arabian Sea (Fig. 9a). To better highlight the possible relationship between the cyclonic anomaly and the precipitation response, in Fig. 10, we decompose the anomalous total wind into its rotational and divergent components at two levels at the top of (850 hPa) and within (900 hPa) the boundary layer. At the higher level, the anomalous wind is clearly dominated by the rotational component, with the divergent component becoming more dominant as the surface is approached. Despite these vertical changes, two features are seen at both heights: 1) the wavelike pattern downstream of the African topography is evident at all levels in the anomalous rotational flow and 2) the anomalous convergence, which is directly linked to and influenced by the anomalous enhanced precipitation over the Arabian Sea, is approximately collocated with the enhanced southerly wind on the eastern flank of the anomalous cyclone. Here we speculate that the cyclonic anomaly in the rotational component is a direct response to the topography removal. Close to the surface, this rotational

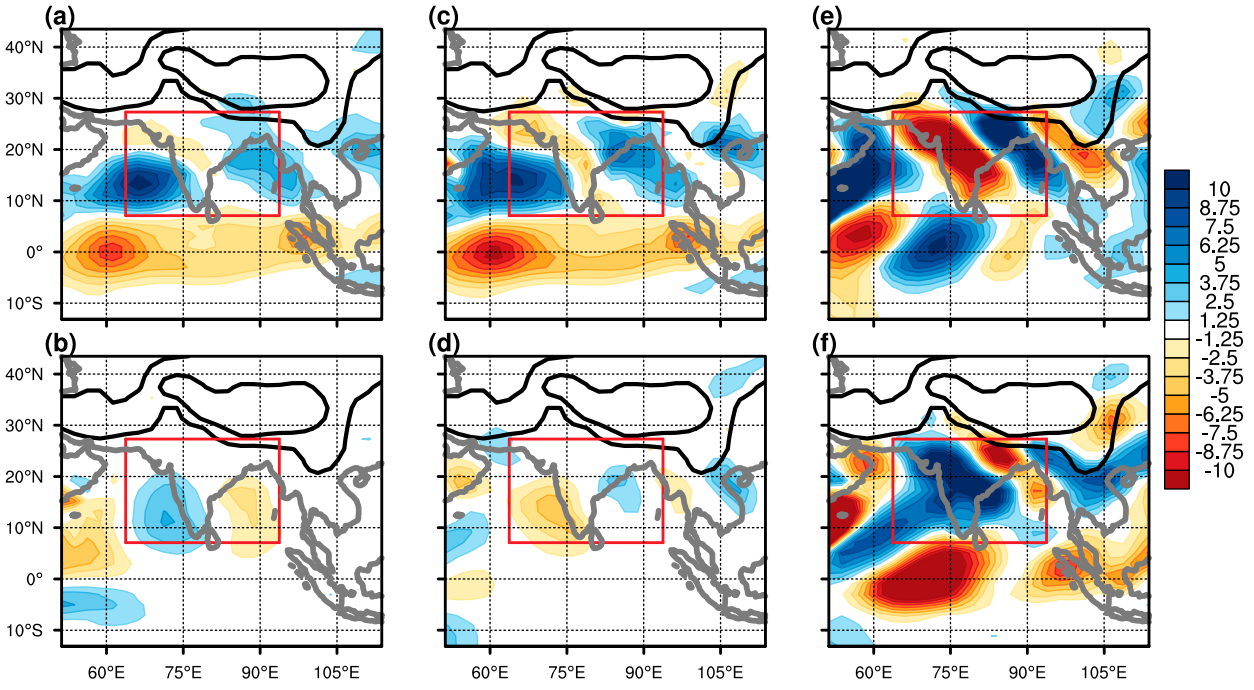

FIG. 7. Anomalous (NoAf–CTL) JJA-average moisture budget: (a) anomalous precipitation; (b) thermodynamic component, (c) convergence, and (d) advection term of the dynamic component; and (e) zonal and (f) meridional dynamic convergence term (mm day^{-1}). Thick black lines indicate the surface pressure in CTL (from 900 to 700 hPa, with an interval of 200 hPa), indicating the location of topography.

response is modified by surface friction and its spatial changes, as the southerly flow approaches the Indian subcontinent, which creates a region of strong meridional wind convergence and enhanced precipitation (Fig. 7).

Therefore, in the following, we focus on understanding dynamical mechanisms responsible for the anomalous rotational component—namely, the lower-level anomalous cyclone over the Arabian Sea—and we focus on the 850-hPa level, where this component has strongest anomalies within the boundary layer. To do so, we consider the full PV dynamics, which includes its sources and sinks, and perform a detailed analysis of its budget. Please note that results would not change, at least qualitatively, if we considered a moisture weighted vertical average (more closely linked to the moisture budget) within the boundary layer.

Ertel's PV, $(1/\rho)(\boldsymbol{\eta}\cdot\nabla\theta)$, is a scalar quantity that expresses both the rotational and stratification features of the fluid. Here, $\boldsymbol{\eta}$ is the 3D absolute vorticity vector, θ the potential temperature, and ρ the density of the fluid. In z coordinates, the PV budget is

$$\frac{D(\mathrm{PV})}{Dt}=\frac{1}{\rho}\mathbf{F}_{\eta}\cdot\nabla\theta+\frac{1}{\rho}\boldsymbol{\eta}\cdot\nabla\dot{\theta}, \tag{2}$$

where $\mathbf{F}_{\eta}$ is the curl of the 3D frictional forcing $\mathbf{F}$ and $\dot{\theta}$ is the heating rate. The first term in the right-hand side of Eq. (2) is the frictional term and the second term is the heating term. This conservation law clearly highlights how PV is materially conserved in the absence of friction and diabatic heating.

RH95 used the PV budget to analyze the dynamics of the Somali cross-equatorial flow. They argued that the change in sign of planetary rotation at the equator would prevent cross-equatorial flow in a stratified fluid, so much so that PV material tendencies are necessary for cross-equatorial flow to be achieved. Particles that retain their negative PV over the Arabian Sea would recirculate back into the SH, with a significant reduction of the moisture flux into the monsoon region. The combination of land–sea contrast in friction, which is enhanced by the African topography, and diabatic heating allows for sufficient positive PV modification and helps maintain the jet in the NH. Removal of topography in their dry model, forced by a prescribed diabatic heating, suggests that without the African topography, PV tendencies would decrease to a point that no significant cross-equatorial flow could be maintained into the Indian monsoon region.

In our simulations, removing the African topography has a significantly less dramatic impact on the cross-equatorial flow than what is discussed in RH95. In fact, the cross-equatorial flow weakens only in its core, close to the region of modified topography. However, we still

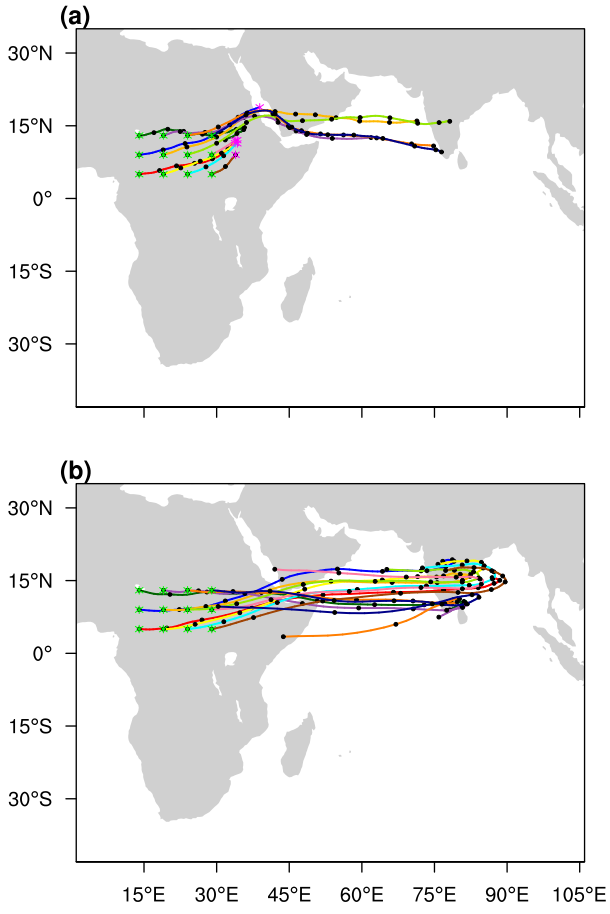

FIG. 8. Forward trajectory analysis for the (a) CTL and (b) NoAf experiments. The green asterisks are the integration-starting points and different colors indicate different integration-starting locations. Particles are chosen to originate from the 850-hPa level.

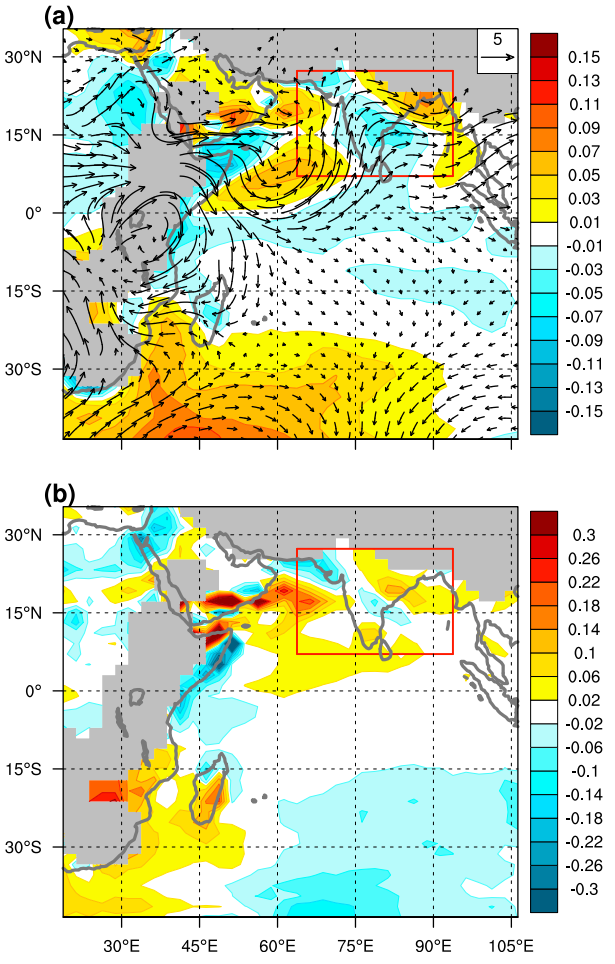

FIG. 9. (a) Anomalous (NoAf–CTL) JJA-average PV [shading, PV unit (PVU), $10^{-6}\,\mathrm{K\,kg^{-1}\,m^2\,s^{-1}}$] and 850-hPa winds (vectors, $\mathrm{m\,s^{-1}}$). (b) Anomalous material PV tendency ($\mathrm{PVU\,day^{-1}}$). The gray shading indicates regions with no data below 850 hPa.

find significant differences in the lower-level flow, and its curvature, downstream of the topography in the CTL and NoAf experiments. In the NoAf experiment, the flow has a stronger meridional component, with anomalous southerlies, compared to that in the CTL experiment, in which the flow is primarily zonally oriented when approaching the Indian subcontinent. This, as discussed above, has a nonnegligible impact on the SAM precipitation. Here, we want to explore if and to what extent these lower-level flow changes can be understood through changes in the PV budget along flow trajectories. To this aim, we perform a PV budget analysis similar to the one done by RH95. One important difference is that in this work we use a full-physics GCM, where diabatic heating is not prescribed but interacts with and depends on the monsoonal circulation. We analyze the overall impact of all terms on the PV budget of the cross-equatorial flow and its downstream extension. In particular, we want to unravel mechanisms responsible for the positive PV anomaly over the Arabian Sea when the African topography is removed.

Figure 9b shows the difference of the JJA mean material PV tendency between the NoAf and CTL experiments at 850 hPa (i.e., the sum of the frictional and heating terms in the PV budget). Please note that changes in the material tendencies at other levels within the boundary layer are of similar magnitude as the ones at 850 hPa (not shown). Caused by the mountain range to the west of the cross-equatorial flow, lateral frictional forces induce positive material PV tendency in the CTL experiment along the particles moving near the African topography. When the African topography is removed, the frictional tendencies to its east decrease, which explains the negative anomalies there. Positive anomalies in PV tendencies are found over the Arabian Sea, in the same broad region of positive PV anomalies. One might

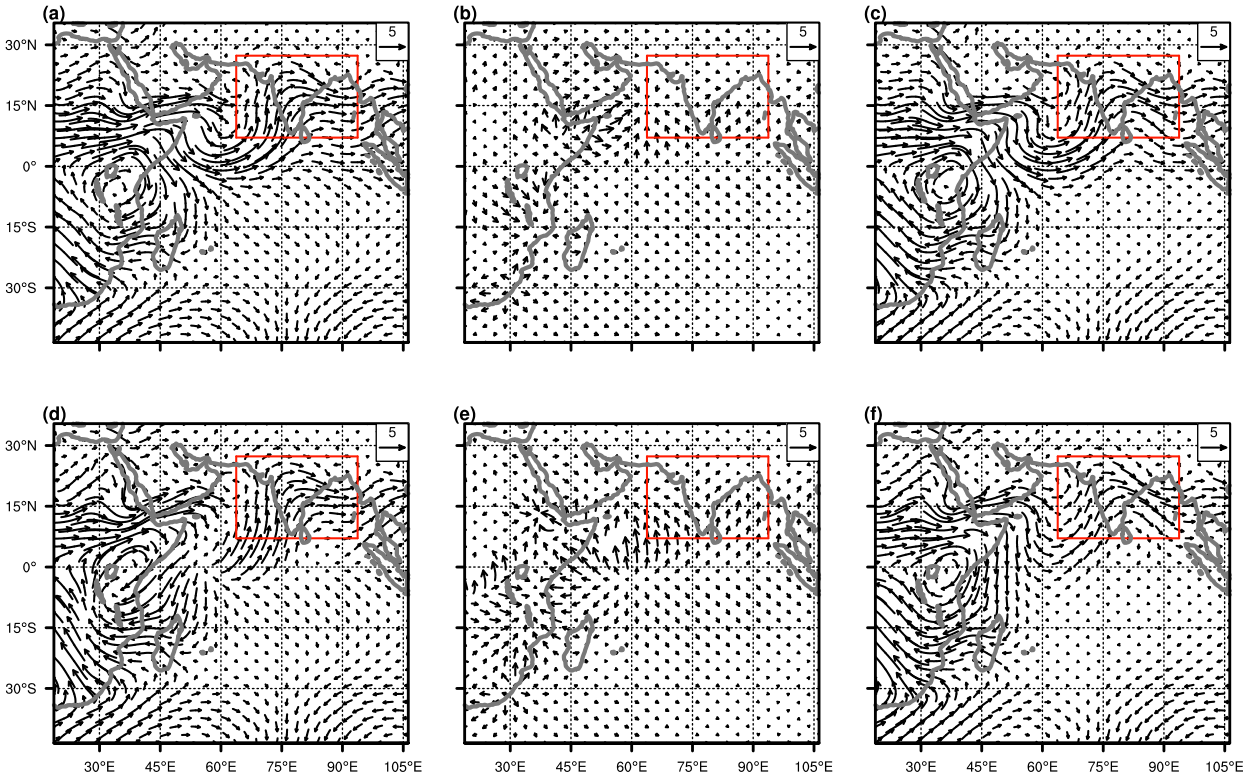

FIG. 10. Anomalous (a),(d) total, (b),(e) divergent, and (c),(f) rotational winds at (top) ~850 and (bottom) ~900 hPa. Please note that these analyses are conducted on hybrid model coordinates.

therefore anticipate that larger PV over the Arabian Sea in the NoAf experiment is primarily due to these positive PV tendencies. However, the tendencies shown in Fig. 9b are material tendencies, which can be directly linked to PV changes only from a Lagrangian perspective, following particle trajectories. That is to say that to understand PV changes over the Arabian Sea, one also needs to consider where particles reaching this region originated from and passed by. To this aim, we analyze the PV budget along backward trajectories for particles with integration-starting points in the Arabian Sea region with largest PV anomalies. In so doing, we account for all factors that can potentially influence PV in the target region, from the particle initial locations, and hence initial planetary vorticity, initial relative vorticity, and material tendencies accumulated along specific paths.

The backward trajectory analysis is calculated in both experiments with particles starting from the region that has largest PV anomaly (Fig. 11). The backward trajectories highlight important differences in the flow between the CTL and NoAf experiments: while in the former the cross-equatorial flow is more coherent and organized, with most of the particles in the Arabian Sea originating from similar latitudes in the SH, in the latter particles appear to originate from different latitudes, from the SH Indian Ocean to near-equatorial Africa. Interestingly, we find that in both experiments particles undergo significant height variations, which influences the material PV tendencies they experience (Figs. 11c,d).

By integrating the material PV tendency along the paths, we can track the anomalous evolution of PV (Fig. 12a) and compute the net PV change along the trajectories.[1] At time 0 h, the PV in the NoAf experiment is larger than that in the CTL experiment for every trajectory (Fig. 12a). This is to be expected since we choose the region of positive PV anomaly as our integration-starting region. However, the PV difference at the integration-ending time of our backward calculation (−240 h) is even more positive. This implies that the larger PV over the Arabian Sea in the NoAf experiment at time 0 h is primarily due to larger values in the initial PV. This can also be seen from Fig. 13, which shows that the averaged total net PV change is larger in the CTL experiment than in the NoAf experiment. If

[1] The offset between the real PV evolution and the accumulated PV evolution integrated from the total material PV tendency is small, so we mainly discuss the calculated PV evolution.

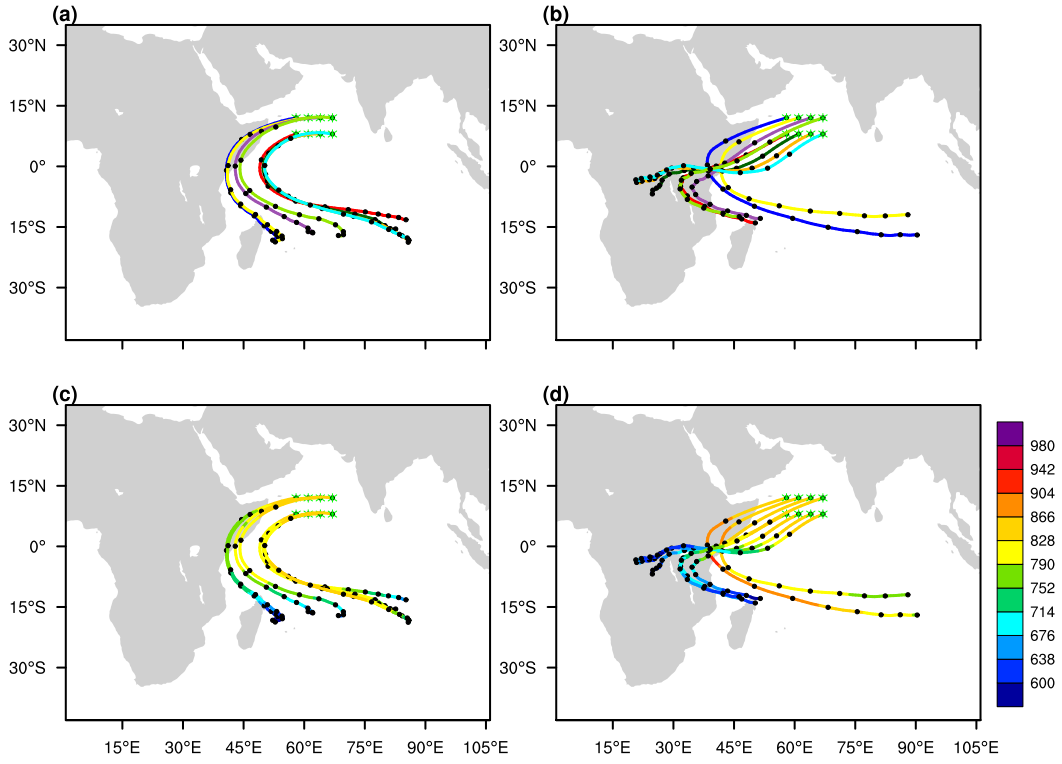

FIG. 11. Backward trajectories in the (a) CTL and (b) NoAf experiments. The green asterisks mark the integration-starting points and different colors indicate different integration-starting locations. Particles are chosen to originate from the 850-hPa level. The integration-starting time is 20 Aug. (c),(d) Trajectories are as in (a),(b), but the color coding indicates the pressure level (hPa) for each point along the trajectories.

this were the dominant effect, the PV anomaly over the Arabian Sea would be negative (anticyclonic) rather than positive (cyclonic). Our results show the opposite, which suggests that the primary difference lies in the initial PV values. More specifically, the positive PV anomaly between the NoAf and CTL experiments over the Arabian Sea is due to the larger (or less negative) initial PV in the NoAf experiment compared to that in the CTL experiment. This is further confirmed in Fig. 14, which shows the time evolution of the latitude along the particle trajectories in the CTL and NoAf experiments and their difference (NoAf-CTL). Because the initial latitudes of the particles are larger (i.e., farther northward) in the NoAf experiment, the particles contain larger initial planetary vorticity and therefore larger initial PV. Similar conclusions can be reached if particles are chosen to originate from a lower level in the backward trajectory calculations.

Please note that the net PV change along trajectories can also be computed following the actual PV evolution along the paths (Fig. 12b). While the PV budget is not completely closed and there exists some residual, the associated error at the beginning of the trajectories is smaller than the difference in initial PV discussed above. Hence, the presence of residuals in the PV budget does not invalidate the main conclusion emerging from our analyses.[2]

The significant differences in the latitude of the initial particle locations between CTL and NoAf are consistent with the changes in the simulated flow, discussed in previous sections. In particular, in the NoAf experiment, the weaker blocking effect by the African topography and the weaker cross-equatorial flow close to the African coast allow for some of the particles to originate farther west and closer to the equator in the SH than what seen in the CTL run. The particles, therefore, have a larger initial planetary vorticity value: this allows them to reach the Arabian Sea with more positive PV, even if the net material PV tendencies along their trajectories are less positive than the one experienced by particles reaching the same location in the CTL experiment. While individual trajectories shown in Figs. 12a and 13 somewhat differ in the relative importance of the

[2] We have also verified that the residual term of the local PV budget (in an Eulerian perspective) is small compared to the material PV tendency (not shown).

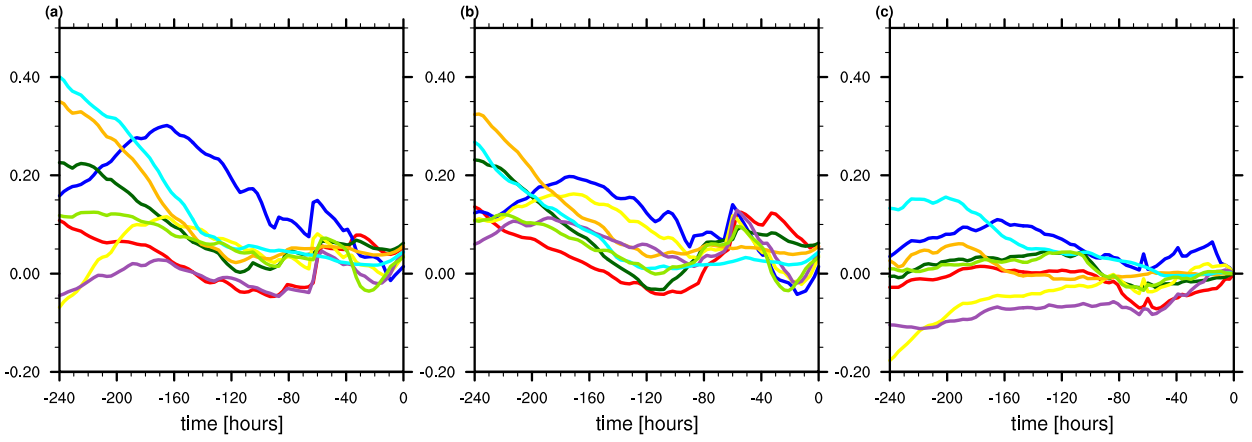

FIG. 12. Anomalous (NoAf–CTL) evolution of PV (a) calculated by integrating the material PV tendency and (b) interpolated along trajectories. (c) The residual (difference) between (a) and (b). Different colors indicate different integration-starting locations, consistent with Figs. 11a and 11b.

initial PV and the material PV tendencies in the resulting PV difference at the end point, most of them do highlight the role of the initial PV difference. Also note that results in Figs. 12a and 13 represent averages for eight different trajectories and, hence, emphasize the general pattern emerging from most trajectories.

Order-of-magnitude calculations also show that the vorticity difference implied by the initial PV difference seen in the backward trajectories (Fig. 12a) and the stratification at those initial locations is of the same order of magnitude of the vorticity difference associated with the differences in starting latitudes in Fig. 14c. This allows us to conclude with some confidence that the positive PV anomaly over the Arabian Sea primarily arises because of differences in the initial location and, hence, planetary vorticity of particles reaching this region in the two experiments. One caveat we want to emphasize here is that we find that the static stability at the beginning of the trajectories (which influences the value of the original PV) is somewhat higher-than-average values in tropical regions. This could result from either a model's artifact due to limitations in the convection scheme or from the fact that particles originate from a region (15°S) where convection is not active and, therefore, characterized by a larger stability.

5. The influence of the Arabian topography

Although our main goal is to focus on the impact of the African topography on the SAM, the Arabian topography is located right to the west of the Indian subcontinent and can be thought of as providing an extension to the African topography. This prompts us to examine further changes in the SAM when the Arabian topography is also removed (Fig. 1c). In the simulation when both African and Arabian topography are removed (NoAfArab), the precipitation in the larger-scale SAM domain increases relative to the CTL experiment (Figs. 5a,c), but decreases slightly relative to the NoAf experiment, primarily in the northwestern portion of the Indian region (Fig. 15a). A moisture budget analysis [Eq. (1)] reveals that this precipitation decrease is associated with a reduction in the dynamic convergence term (Fig. 15).

While the PV anomaly over the Arabian Sea is stronger in the NoAfArab experiment than in the NoAf experiment (Figs. 9 and 16), the precipitation response has opposite sign (Fig. 15a). That is, the precipitation increase relative to the CTL run on the eastern flank of the cyclonic anomaly over the Arabian Sea is smaller when both the Arabian and African topography are removed than when the African topography is removed in isolation. This appears to be due to the fact that the southerly flow on the eastern flank of the stronger PV anomaly, associated with anomalous meridional convergence relative to the CTL experiment, does not increase in the NoAfArab experiment relative to the NoAf experiment. This can occur because PV is not only influenced by the absolute vorticity but, also, by the atmospheric stability. Changes in the latter can induce changes in the PV field, without changes in the absolute vorticity. Additionally, changes in relative vorticity are not necessarily correlated to changes in the southerly flow on the eastern flank of the PV positive anomaly. Therefore, the small changes in PV between the NoAf and NoAfArab experiments are not easily related to wind circulation patterns, and associated precipitation changes, near the Indian region. This highlights the complexity of the circulation response to changes in topography in a full-physics GCM.

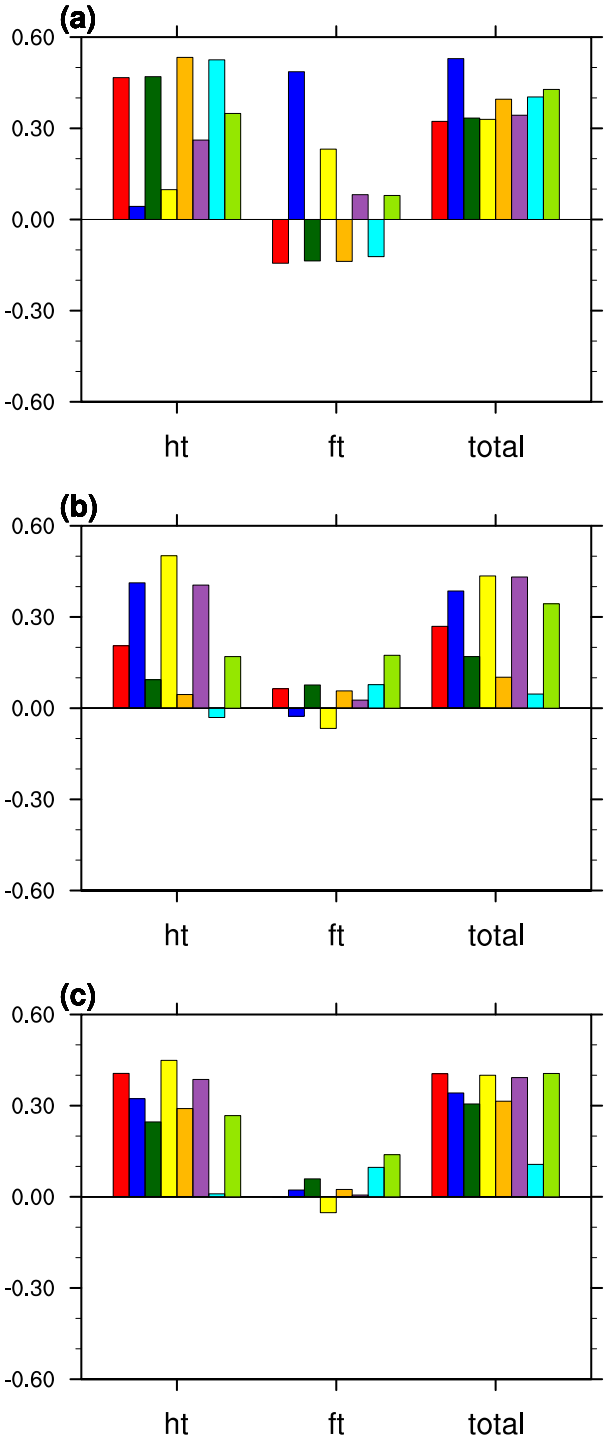

FIG. 13. Net PV change along the 10-day trajectories for the (a) CTL, (b) NoAf, and (c) NoAfArab experiments. Abbreviations "ht," "ft," and "total" indicate the heating, the frictional, and the total (heating + frictional) material PV tendencies, respectively. Different colors indicate different integration-starting locations, consistent with Figs. 11a and 11b.

Despite not necessarily providing a direct link to understanding precipitation changes, it is still of interest to analyze mechanisms behind the PV increase over the Arabian Sea when the Arabian topography is removed. Therefore, we compute the PV budget following particle trajectories. The backward trajectories are similar to the ones in the NoAf experiment (not shown). The difference in the initial particle location, which was critical in explaining differences between the NoAf and CTL experiments, does not play a significant role here. This means that removing the Arabian topography does not modify substantially the trajectories of particles that reach the Arabian Sea in the region of largest PV anomaly. This suggests that accumulated PV material tendencies have to be larger in the NoAfArab experiment than in the NoAf one to explain the positive PV anomaly between the two experiments. This is confirmed in Fig. 13c, which also shows that the larger material PV modification arises from the larger heating term, rather than changes in the frictional term.

In summary, these results show how the Arabian topography has a relative small impact on the SAM precipitation response and only slightly modifies the response to the removal of the African topography. This might be due to the smaller height and range of this topographical feature, as well as its location: being farther north than the African topography, the Arabian topography likely has a smaller interaction with the cross-equatorial flow.

6. Conclusions

The precise role that the African topography plays on the structure and intensity of the SAM cross-equatorial flow and precipitation still remains debated. While it is widely accepted in the literature that the African topography helps to spatially confine the cross-equatorial flow and to enhance the SAM precipitation, recent studies show how the SAM precipitation increases rather than decreasing in numerical experiments when the African topography is removed. Here, we perform similar GCM experiments with modified topography and we provide a more comprehensive and quantitative discussion of the impact of the topography on the monsoonal lower-level flow and precipitation.

In simulations with a full-physics GCM, when the African topography is removed, the SAM precipitation increases even if the cross-equatorial flow weakens. We find that in the absence of the blocking effect of the African topography, westerly winds strengthen over the eastern African coast. Previous studies attributed the precipitation increase in the absence of the African topography to the strengthening of the westerly

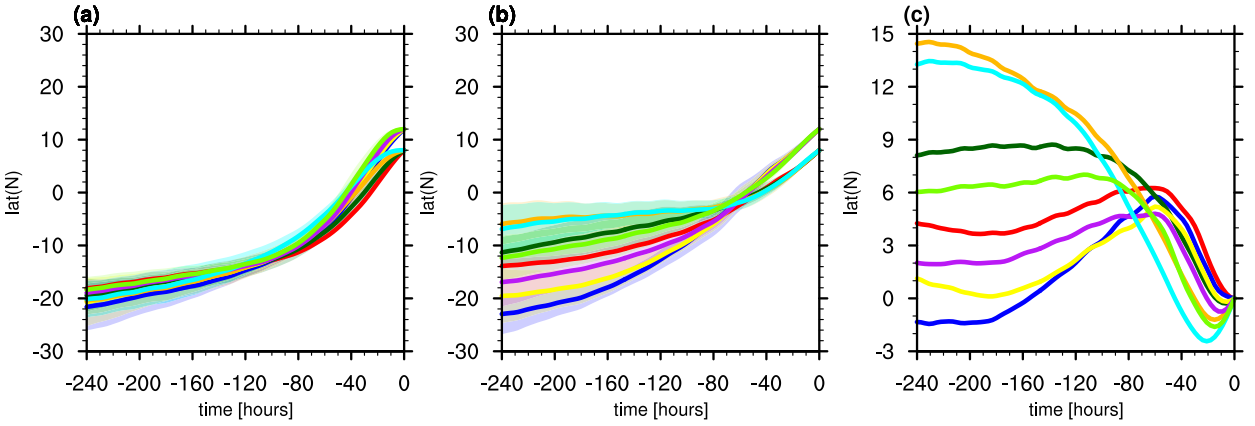

FIG. 14. Evolution of latitude along the trajectories starting from the same locations as those in Fig. 11 for (a) CTL, (b) NoAf, and (c) difference between the two (NoAf–CTL). In (a),(b), the thick lines show the mean and the shading shows the spread (two standard deviations) in the eight trajectories with eight different integration-starting times.

winds, and associated moisture convergence, as the zonal flow approaches the Indian subcontinent. In our simulations, however, enhanced westerlies do not extend over the Arabian Sea, and stronger precipitation arises because of stronger meridional, rather than zonal, convergence. This enhanced meridional convergence is in turn associated with anomalous southerly flow on the eastern flank of a cyclonic wind, or positive PV, anomaly over the Arabian Sea.

PV budget analyses along particle trajectories are being conducted to explain mechanisms giving rise to this cyclonic, or positive PV, anomaly. It is shown that

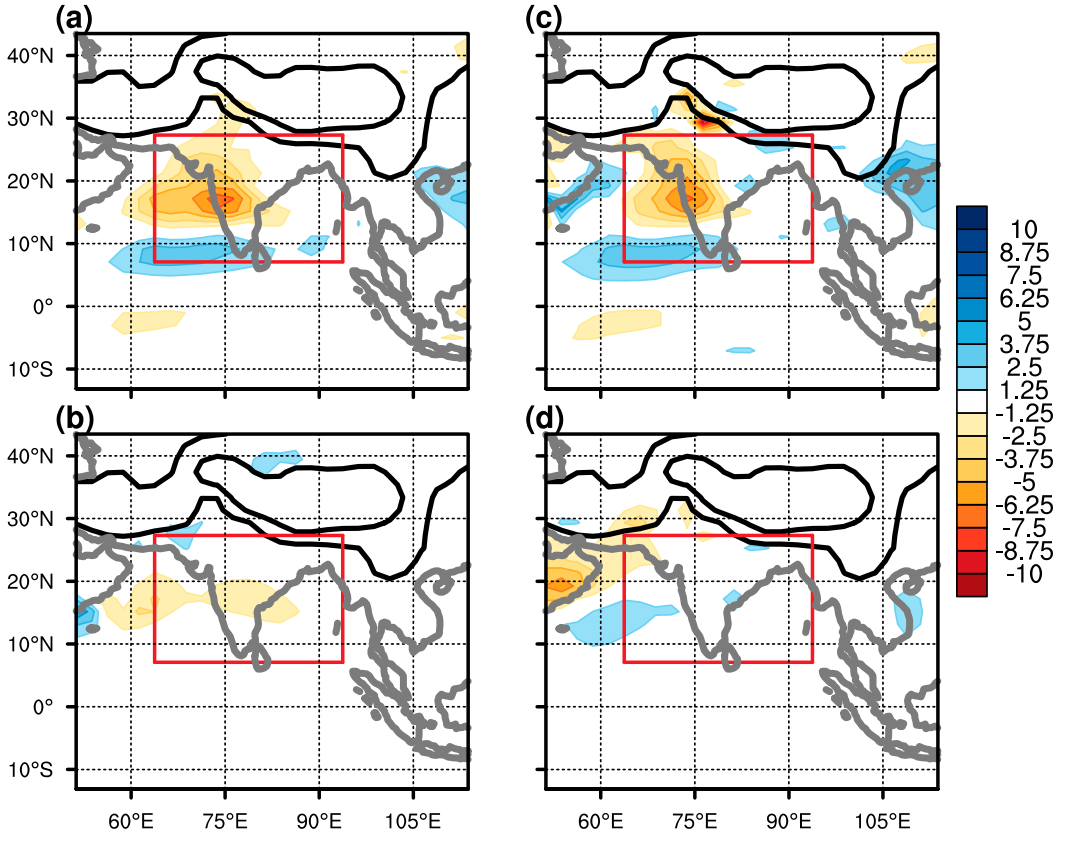

FIG. 15. As in Figs. 7a–d, but for the difference between the NoAfArab and NoAf experiments.

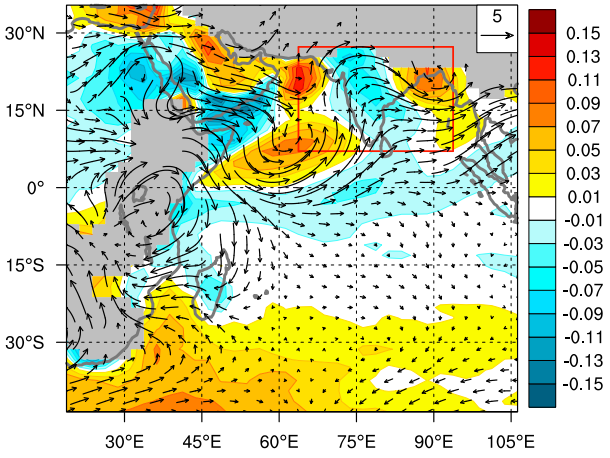

FIG. 16. As in Fig. 9a, but for the PV difference between the NoAfArab and CTL experiments.

particles over the Arabian Sea have higher PV in the NoAf experiment relative to those in the CTL experiment not because they experience more positive material PV tendencies along their paths but, rather, because they tend to originate from higher latitudes and, therefore, carry with them higher values of initial planetary vorticity. Weaker cross-equatorial flow and weaker blocking effect (i.e., stronger westerly wind) in the absence of the African topography allow for particles originating from near-equatorial Africa or over the near-equatorial SH Indian Ocean to reach the monsoon region. Because of the larger PV, the flow over the Arabian Sea has a stronger southerly component to the west of India and, associated with it, stronger moisture convergence and precipitation in the NoAf experiment.

We also conduct and discuss an experiment where the Arabian topography is removed in addition to the African topography. Despite inducing interesting and nonintuitive changes in the circulation and precipitation fields, the Arabian topography is found to have only a very modest influence on the monsoon, consistent with its smaller extent, height, and northward position relative to the African topography.

In our simulations, we do not consider the ocean response to the circulation changes, in that SSTs are kept fixed and the same in all experiments. The ocean–atmosphere coupling can have important impacts on the mechanisms here discussed. For instance, the reduction of the cross-equatorial flow as the African topography is removed would reduce upwelling and increase SSTs. Similarly, changes in wind strength could induce further SST changes through evaporation, which in turn would influence the precipitation response. These effects will be explored in future studies with experiments in a slab ocean or fully coupled GCM. The sensitivity of our results to changes in model physics and horizontal resolution is also not explored in this study. However, similar experiments conducted with different GCMs (Chakraborty et al. 2002, 2006, 2009; Slingo et al. 2005) show responses in the SAM precipitation and circulation patterns that are in qualitative, if not quantitative, agreement with the ones reported here. This suggests that the large-scale features that are the focus of our study are not an artifact of the model physics and configuration and have some generality.

Unlike more idealized work, which has attempted to consider the impact of topography and diabatic heating in isolation on the monsoonal flow, here we use a comprehensive GCM, where the distribution of diabatic heating is itself part of the response and dependent on the monsoonal circulation. Therefore, as the lower boundary is modified (here through changes in topography) the precipitation distribution can respond in ways not predicted by more idealized studies. As the topography is removed, changes in the resulting circulation will induce changes in the diabatic heating, which in turn will affect the PV of the monsoonal cross-equatorial flow and larger-scale circulation. While making causality harder to assess, this approach has the advantage of being energetically and dynamically consistent. In particular, it allows us to show how the Indian monsoon is significantly less sensitive to the presence of the African topography and a topographically confined Somali jet than what commonly thought: in fact, while having a quantitative impact on the structure of the Somali jet, the removal of the African topography does not modify in any significant way any of the major features of the simulated SAM, such as its position, strength, and seasonality.

In this respect, this work is consistent with emerging theories of monsoons, which view these tropical circulations as regional manifestations of the seasonal cycle of the tropical Hadley circulation (e.g., Gadgil 2003; Bordoni and Schneider 2008) rather than large-scale sea-breeze circulations driven by local forcing. By shedding insight into the response of the SAM to modified topography, and resulting flow–precipitation interactions, this study might help to better constrain the influence of radiative and land surface forcing on the monsoon on different time scales.

Acknowledgments. This work was partially supported by the Caltech Terrestrial Hazard and Reporting (THOR) Center. We thank Brian Hoskins, an anonymous reviewer, and Ming Cai for their helpful review and insightful suggestions. We also thank Zhiming Kuang, Ian Eisenman, and Olivier Pauluis for the helpful

discussions. The numerical simulations and analyses were conducted on the Caltech's Division of Geological and Planetary Sciences CITerra high-performance computing cluster.

REFERENCES

Anderson, D. L. T., 1976: The low-level jet as a western boundary current. *Mon. Wea. Rev.*, **104**, 907–921, doi:10.1175/1520-0493(1976)104<0907:TLLJAA>2.0.CO;2.

Anderson, J., and Coauthors, 2004: The new GFDL global atmosphere and land model AM2–LM2: Evaluation with prescribed SST simulations. *J. Climate*, **17**, 4641–4673, doi:10.1175/JCLI-3223.1.

Boos, W. R., and K. A. Emanuel, 2009: Annual intensification of the Somali jet in a quasi-equilibrium framework: Observational composites. *Quart. J. Roy. Meteor. Soc.*, **135**, 319–335, doi:10.1002/qj.388.

——, and Z. Kuang, 2010: Dominant control of the South Asian monsoon by orographic insulation versus plateau heating. *Nature*, **463**, 218–222, doi:10.1038/nature08707.

Bordoni, S., and T. Schneider, 2008: Monsoons as eddy-mediated regime transitions of the tropical overturning circulation. *Nat. Geosci.*, **1**, 515–519, doi:10.1038/ngeo248.

Chakraborty, A., R. S. Nanjundiah, and J. Srinivasan, 2002: Role of Asian and African orography in Indian summer monsoon. *Geophys. Res. Lett.*, **29**, 1989, doi:10.1029/2002GL015522.

——, ——, and ——, 2006: Theoretical aspects of the onset of Indian summer monsoon from perturbed orography simulations in a GCM. *Ann. Geophys.*, **24**, 2075–2089, doi:10.5194/angeo-24-2075-2006.

——, ——, and ——, 2009: Impact of African orography and the Indian summer monsoon on the low-level Somali jet. *Int. J. Climatol.*, **29**, 983–992, doi:10.1002/joc.1720.

Clement, A. C., A. Hall, and A. J. Broccoli, 2004: The importance of precessional signals in the tropical climate. *Climate Dyn.*, **22**, 327–341, doi:10.1007/s00382-003-0375-8.

Findlater, J., 1969: A major low-level air current near the Indian Ocean during the northern summer. *Quart. J. Roy. Meteor. Soc.*, **95**, 362–380, doi:10.1002/qj.49709540409.

Gadgil, S., 2003: The Indian monsoon and its variability. *Annu. Rev. Earth Planet. Sci.*, **31**, 429–467, doi:10.1146/annurev.earth.31.100901.141251.

Halpern, D., and P. M. Woiceshyn, 2001: Somali jet in the Arabian Sea, El Niño, and India rainfall. *J. Climate*, **14**, 434–441, doi:10.1175/1520-0442(2001)014<0434:SJITAS>2.0.CO;2.

Held, I. M., and B. J. Soden, 2006: Robust responses of the hydrological cycle to global warming. *J. Climate*, **19**, 5686–5699, doi:10.1175/JCLI3990.1.

Hoskins, B. J., and M. J. Rodwell, 1995: A model of the Asian summer monsoon. Part I: The global scale. *J. Atmos. Sci.*, **52**, 1329–1340, doi:10.1175/1520-0469(1995)052<1329:AMOTAS>2.0.CO;2.

Krishnamurti, T. N., J. Molinari, and H. L. Pan, 1976: Numerical simulation of the Somali jet. *J. Atmos. Sci.*, **33**, 2350–2362, doi:10.1175/1520-0469(1976)033<2350:NSOTSJ>2.0.CO;2.

Li, C., and M. Yanai, 1996: The onset and interannual variability of the Asian summer monsoon in relation to land–sea thermal contrast. *J. Climate*, **9**, 358–375, doi:10.1175/1520-0442(1996)009<0358:TOAIVO>2.0.CO;2.

Meehl, G. A., 1994: Coupled land–ocean–atmosphere processes and South Asian monsoon variability. *Science*, **266**, 263–267, doi:10.1126/science.266.5183.263.

Nie, J., W. R. Boos, and Z. Kuang, 2010: Observational evaluation of a convective quasi-equilibrium view of monsoons. *J. Climate*, **23**, 4416–4428, doi:10.1175/2010JCLI3505.1.

Paegle, J., and J. E. Geisler, 1986: The effect of East African topography on flow driven by zonally symmetric forcing. *J. Atmos. Sci.*, **43**, 1862–1872, doi:10.1175/1520-0469(1986)043<1862:TEOEAT>2.0.CO;2.

Rodwell, M. J., and B. J. Hoskins, 1995: A model of the Asian summer monsoon. Part II: Cross-equatorial flow and PV behavior. *J. Atmos. Sci.*, **52**, 1341–1356, doi:10.1175/1520-0469(1995)052<1341:AMOTAS>2.0.CO;2.

Sashegyi, K. D., and J. E. Geisler, 1987: A linear model study of cross-equatorial flow forced by summer monsoon heat sources. *J. Atmos. Sci.*, **44**, 1706–1722, doi:10.1175/1520-0469(1987)044<1706:ALMSOC>2.0.CO;2.

Slingo, J., H. Spencer, B. Hoskins, P. Berrisford, and E. Black, 2005: The meteorology of the western Indian Ocean, and the influence of the East African Highlands. *Philos. Trans. Roy. Soc. London*, **A363**, 25–42, doi:10.1098/rsta.2004.1473.

Smith, T. M., R. W. Reynolds, R. E. Livezey, and D. C. Stokes, 1996: Reconstruction of historical sea surface temperatures using empirical orthogonal functions. *J. Climate*, **9**, 1403–1420, doi:10.1175/1520-0442(1996)009<1403:ROHSST>2.0.CO;2.

Walker, J. M., S. Bordoni, and T. Schneider, 2015: Interannual variability in the large-scale dynamics of the South Asian summer monsoon. *J. Climate*, **28**, 3731–3750, doi:10.1175/JCLI-D-14-00612.1.

Webster, P. J., 1987: The elementary monsoon. *Monsoons*, J. S. Fein and P. L. Stephens, Eds., Wiley, 3–32.

Wu, G., Y. Liu, B. He, Q. Bao, A. Duan, and F.-F. Jin, 2012: Thermal controls on the Asian summer monsoon. *Sci. Rep.*, **2**, 404, doi:10.1038/srep00404.